IEEE Open Journal of
Vehicular Technology

Received 11 January 2022; accepted 16 January 2022. Date of publication 21 January 2022;
date of current version 17 February 2022. The review of this article was coordinated by Editor Zhaocheng Wang.

Digital Object Identifier 10.1109/OJVT.2022.3144570

Phase Difference Based Precise Indoor Tracking of Common Mobile Devices Using an Iterative Holographic Extended Kalman Filter

STEFAN BRÜCKNER [1], ERIK SIPPEL [1], MELANIE LIPKA [2], JOHANNA GEISS [1] (Graduate Student Member, IEEE), AND MARTIN VOSSIEK [1] (Fellow, IEEE)

[1]Institute of Microwaves and Photonics, Friedrich-Alexander University Erlangen-Nuremberg, 91058 Erlangen, Germany
[2]IIS, Fraunhofer-Gesellschaft zur Förderung der angewandten Forschung eV, 91058 Erlangen, Germany

CORRESPONDING AUTHOR: STEFAN BRÜCKNER (e-mail: stefan.brueckner@fau.de)

This work was supported by the German Research Foundation under Grant DFG VO 1453/35-1.

ABSTRACT The 3D indoor localization of low-cost standard mobile devices represents an important research topic. Since the implementation of ultra-wideband localization systems requires elaborated hardware, a localization concept based on phase-difference-of-arrival (PDOA) evaluation of narrow band communication signals at spatially distributed antennas is favorable in many applications. Typically, PDOA measurements are used to estimate the angle-of-arrival (AOA) at several receivers, which are then combined via multiangulation. However, AOA estimation requires far field conditions, thereby limiting measurement sensitivity, and distorts measurements in a non linear fashion. To overcome these limitations, this paper proposes the iterative holographic extended Kalman filter (IHEKF), which directly evaluates the phase differences between spatially distributed antenna pairs. The IHEKF requires neither a specific waveform nor emitter–receiver synchronization and, therefore, represents a good candidate for localization within communication systems such as 5G/6G. Since the evaluation of phase differences is affected by phase ambiguity, the IHEKF is designed so that closely spaced antenna pairs are evaluated first and then more distant antennas are included successively to improve accuracy. The IHEKF's capabilities are demonstrated via a 24 GHz narrow band measurement setup with strong multipath propagation, providing outstanding localization accuracy in the millimeter range without consuming any notable RF signal bandwidth.

INDEX TERMS Array signal processing, incoherent measurements, Kalman filter, localization, near-field, PDOA, radar.

I. INTRODUCTION

In recent years, wireless localization has attained constantly rising popularity. The continuously increasing appearance of smartphones, RFID tags, and other devices with wireless communication has initiated countless new applications, particularly for localization using electromagnetic waves [1]–[4]. For many of these, global positioning systems are neither accurate nor reliable enough, or they are simply not available, such as in indoor applications. Therefore, there has been extensive scientific effort to advance indoor localization methods, as summarized in [2] and [4].

The most widely used localization techniques are received-signal-strength (RSS) [5], angle-of-arrival (AOA) [6], time-of-arrival (TOA) [7], time-difference-of-arrival (TDOA) [8], and round-trip-time-of-flight (RTOF) [9]. received-signal-strength (RSS)-based positioning systems evaluate solely information about the received signal power, emitted by a beacon and received by multiple base stations, to calculate the beacon's position. It may be used with a simple and inexpensive hardware setup and does not require any synchronization or a specific signal shape. However, only moderate localization accuracy can be achieved, unless a precise signal map is

prerecorded [10] or the signal propagation model can be suitably adapted in real time [5]. More accurate results are realized by evaluating the time-of-arrival (TOA) of a wave, emitted by a beacon and received by a stationary receiver. Therefore, each emitter–receiver pair has to be synchronized [11]. Since reliable beacon–receiver synchronization is very challenging, many systems only evaluate the time-difference-of-arrival (TDOA) [12]. Alternatively, the round-trip-time-of-flight (RTOF) can be measured. For this purpose, a station emits a wave and measures the time until the wave, which is repeated by a beacon in a predefined manner, arrives back at the station. Here, no synchronization is necessary, but precise knowledge of the delay caused by the beacon is required. Independent of the implementation concept, the accuracy of all time-based localization methods depends on the utilized bandwidth [13]. Therefore, ultra-wideband (UWB) represents the current state of the art concerning highly accurate indoor localization [14], [15], which results in millimeter-range accuracy by employing bandwidth of several gigahertz [16]–[18]. However, implementing measurement systems with high bandwidth involves several drawbacks that hinder accurate positioning and increase hardware complexity, including the need for very high sample rates, sensitivity to timing errors and clock jitter, and frequency- and direction-dependent antenna phase centers [18], [19]. Most importantly, the available bandwidth is restricted by governmental restrictions, and nearly all existing communication standards do not allow the excessive use of bandwidth.

Instead of evaluating the frequency dependency of the arriving signal phase at a single antenna, the spatial distribution of the wave field can be coherently recorded with an antenna array as a so-called hologram [20], [21]. Afterwards, the beacon can be located via the phase distribution within the measured holograms at several antenna arrays. In standard communication systems, the beacon usually operates incoherently in respect to the receiving array. In this case, only hologram phase differences, i.e. the PDOA, can be evaluated. In contrast to systems that measure signal propagation time (TOA, TDOA, and RTOF), the localization accuracy is therefore not determined by the signal's bandwidth. Instead, PDOA localization accuracy primarily depends on array aperture size, operating frequency, and beacon-receiver distance. Accurate PDOA based localization results can thus be achieved using simple narrow band hardware [13]. The most established PDOA evaluation concept is the AOA determination [6]. Here, the angle of an impinging plane wave is calculated via the relative phase measurements in a planar antenna array; In this way, closely spaced antennas enable unambiguous angle estimation, while the estimation with more distant antennas is precise. [22] Afterwards the position of the transmitter is derived using multiangulation [23], [24]. Unfortunately, the detour of first estimating the angle at each array and then combining the estimations into one position causes high computational effort, constrains positioning into the far field of the arrays, and loses information during the AOA estimation, as discussed in [25]. To skip this intermediate step of calculating the AOA, the holographic extended Kalman filter (HEKF), introduced in [26], directly compares the phase differences in the measured hologram with the expected phase differences to localize the transmitter. Here, the drawbacks of AOA estimation with subsequent multiangulation, namely the high computational effort and restriction to the far field, are eliminated. Meanwhile, the benefits of PDOA, namely high accuracy, independence of the signal shape, low bandwidth, high measurement rate, and relaxed synchronization requirements, are retained. The HEKF in [26] enabled a significant accuracy improvement of PDOA-based localization, but it represents an immature approach, which evaluates all phase differences that can be calculated between the antennas at each array in every update step at once. Consequently, the HEKF is susceptible to converge to a false position as soon as only one evaluated phase difference causes an error, which cannot be resolved unambiguously due to the 2π periodicity of the phase differences. It is therefore either only suitable for small arrays, thereby limiting measurement sensitivity [13], or it requires very high update rates to cope with the phase ambiguity of large arrays in a recursive manner. Thus, in contrast to the AOA estimation, the unambiguity information of closely spaced antennas is not utilized. Furthermore, the processing of all difference phases in the HEKF contains much redundant information and increases computational effort, which stands in conflict with the required high update rates.

To eliminate these drawbacks, this paper proposes the IHEKF, which enables using both the unambiguity information of closely spaced antenna and the exactness of distant antennas while being more computationally efficient. For this purpose, the IHEKF update is designed so that closely spaced antenna pairs, which provide unambiguous position information even for large beacon position updates, are first evaluated, and then more distant antennas, which improve localization accuracy due to their high measurement sensitivity [13], are added successively. The IHEKF is derived from ground up, thereby investigating the requirement for the filter to converge to the optimal solution. The algorithm is validated by indoor measurements in a 24 GHz setup with large receiver arrays, demonstrating the IHEKF's capability to resolve phase ambiguity issues and yielding a localization accuracy in the millimeter range.

The remaining paper is organized as follows. First, in Section II, the concept, the setup and the advantages of the localization method are described. In Section III, the system model is introduced, and the algorithm is derived from scratch in Section IV. In Section V, an experimental evaluation and verification of the algorithm is provided. Finally, a conclusion finishes this paper.

II. LOCALIZATION CONCEPT AND SYSTEM SETUP

In recent years, there has been a tremendous scientific effort to advance ultra-wideband (UWB)–based indoor positioning, achieving record accuracy in the millimeter range

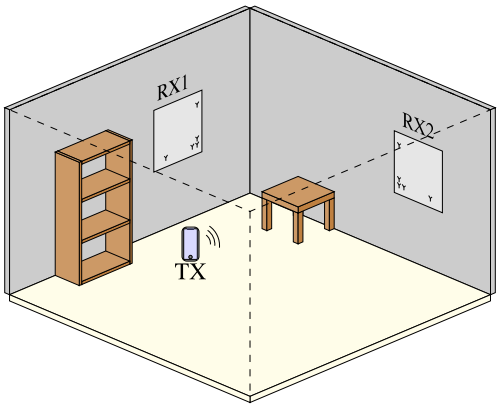

FIGURE 1. Illustration of an exemplary indoor measurement setup of the proposed localization concept. The basic structure of the system and receiver setup is depicted in Fig. 2.

using measurement setups with a bandwidth of several gigahertz [8], [18]. Though the achieved localization accuracy is impressive, a widespread implementation in standard mobile devices appears to be unlikely, especially due to the necessity for highly accurate time synchronization. In contrast, 3D localization systems, which evaluate the PDOA at several receiver arrays, as in the measurement setup shown in Fig. 1, only require very coarse synchronization between receivers, since the necessary synchronization precision only depends on the dynamics of the expected movement and is not related to the signal's propagation time. This advantage makes PDOA approaches particularly suitable for localization within current and future communication standards such as 5G/6G. The possibility of exchanging UWB measurements with PDOA measurements for highly accurate indoor localization was examined in [13]. To obtain a rule of thumb for the direct comparison of PDOA and TOA systems, the bandwidth–dependent measurement sensitivity of TOA systems and the position-dependent phase difference evaluation of PDOA systems was analyzed. For a PDOA-based localization system with the operating frequency f_0, the aperture size L_R, and a maximum beacon–receiver distance d_max, this comparison results in the equivalent bandwidth

$$B_\mathrm{PDOA,eq} = f_0 \frac{L_\mathrm{R}}{d_\mathrm{max}}, \tag{1}$$

which depicts an approximated counterpart to the bandwidth of a 3D TOA-based indoor positioning system. Inspecting (1) reveals that PDOA–based localization systems are superior when the localized beacon is at close range (e.g. < 10 m) and receiver arrays are used that are notably larger than the signal wavelength, which is easily achievable for millimeter waves.

To enable this PDOA-based 3D localization via receivers with large apertures, the IHEKF is proposed in this paper.

The IHEKF directly evaluates the phase difference measurements between the antenna pairs. Since these phase differences are 2π-ambiguous, the IHEKF starts with an evaluation of closely spaced antenna pairs (e.g. the three antennas arranged in the small triangle of each receiver in Fig. 1) to improve the estimation of the beacon's position and then iteratively involves more distant antennas (e.g. the two distant antennas of each receiver in 1) into the state estimation.

As illustrated in the basic system structure in Fig. 2, the beacon might consist of a mixer, which converts any arbitrary narrow band signal to the operating frequency, and an antenna, which transmits the signal. Hence, virtually no requirements on the beacon are necessary for the proposed localization method. The beacon's signal is received by the spatially distributed antennas at each receiver. There, the signals are coherently mixed into the baseband, enabling the evaluation of the phase differences between each antenna pair within this receiver. Similar to the beacon, the receivers do not require any elaborated hardware, and widespread standard receiver hardware can hence be employed for the proposed localization concept. In this paper, a setup with a single beacon is considered, thereby restricting applicability at first glance. However, in multiple-input multiple-output (MIMO) systems, the phase data can be directly extracted from the necessary channel matrix estimation [27], thereby enabling multi–user operation. In summary, the proposed IHEKF is an ideal candidate for highly accurate PDOA-based localization within established communication standards such as WLAN, Bluetooth, and particularly the 5G/6G mobile communication standards, which anyway use large receiver arrays for massive MIMO-based communication [28].

III. SYSTEM MODEL

A. MOVEMENT MODEL

Since this contribution mainly proposes a novel measurement system, arbitrary movement models can be assumed. In this article, the constant velocity model is used.

At the kth measurement, the beacon is located at the position

$$\vec{p}_{\mathrm{B},k} = (x_{\mathrm{B},k}, y_{\mathrm{B},k}, z_{\mathrm{B},k})^\mathsf{T} \tag{2}$$

with the velocity

$$\vec{v}_{\mathrm{B},k} = (\dot{x}_{\mathrm{B},k}, \dot{y}_{\mathrm{B},k}, \dot{z}_{\mathrm{B},k})^\mathsf{T}. \tag{3}$$

With the constant velocity model and the time between two measurements T_s, the current state, consisting of $\vec{p}_{\mathrm{B},k}$ and $\vec{v}_{\mathrm{B},k}$, is obtained using the previous state $\vec{p}_{\mathrm{B},k-1}$ and $\vec{v}_{\mathrm{B},k-1}$ as

$$\begin{pmatrix} \vec{p}_{\mathrm{B},k} \\ \vec{v}_{\mathrm{B},k} \end{pmatrix} = \boldsymbol{F} \begin{pmatrix} \vec{p}_{\mathrm{B},k-1} \\ \vec{v}_{\mathrm{B},k-1} \end{pmatrix} + \boldsymbol{G}\vec{n}_{\mathrm{B},k} \tag{4}$$

$$\begin{pmatrix} x_{\mathrm{B},k} \\ y_{\mathrm{B},k} \\ z_{\mathrm{B},k} \\ \dot{x}_{\mathrm{B},k} \\ \dot{y}_{\mathrm{B},k} \\ \dot{z}_{\mathrm{B},k} \end{pmatrix} = \begin{bmatrix} 1 & 0 & 0 & T_s & 0 & 0 \\ 0 & 1 & 0 & 0 & T_s & 0 \\ 0 & 0 & 1 & 0 & 0 & T_s \\ 0 & 0 & 0 & T_s & 0 & 0 \\ 0 & 0 & 0 & 0 & T_s & 0 \\ 0 & 0 & 0 & 0 & 0 & T_s \end{bmatrix} \begin{pmatrix} x_{\mathrm{B},k-1} \\ y_{\mathrm{B},k-1} \\ z_{\mathrm{B},k-1} \\ \dot{x}_{\mathrm{B},k-1} \\ \dot{y}_{\mathrm{B},k-1} \\ \dot{z}_{\mathrm{B},k-1} \end{pmatrix}$$

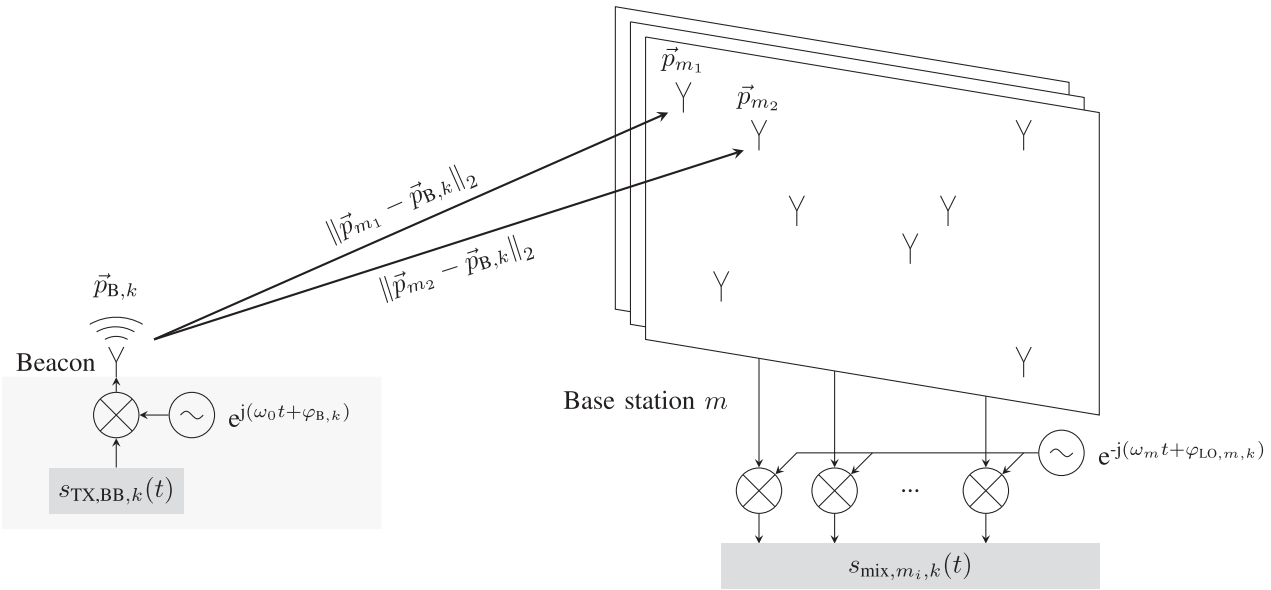

FIGURE 2. Illustration of the basic system setup with the beacon and three receivers, including the antennas and the signal chain at one receiver.

$$+\begin{bmatrix} \frac{T_s^2}{2} & 0 & 0 \\ 0 & \frac{T_s^2}{2} & 0 \\ 0 & 0 & \frac{T_s^2}{2} \\ T_s & 0 & 0 \\ 0 & T_s & 0 \\ 0 & 0 & T_s \end{bmatrix} \begin{pmatrix} n_{\dot{x}_{\mathrm{B},k}} \\ n_{\dot{y}_{\mathrm{B},k}} \\ n_{\dot{z}_{\mathrm{B},k}} \end{pmatrix}, \tag{5}$$

where the velocity noise $n_{\dot{x}_{\mathrm{B},k}}, n_{\dot{y}_{\mathrm{B},k}}, n_{\dot{z}_{\mathrm{B},k}} \sim \mathcal{N}(0, \sigma_a^2)$ is assumed to occur as a constant acceleration between successive states with zero mean and the standard deviation σ_a.

B. MEASUREMENT MODEL

In this section, the measurement model, depicted in Fig. 2, is introduced. The beacon emits the signal

$$s_{\mathrm{B},k}(t) = A \cdot s_{\mathrm{TX,BB},k}(t) e^{j(\omega_0 t+\varphi_{\mathrm{B},k})} \tag{6}$$

with amplitude A, an arbitrary baseband signal $s_{\mathrm{TX,BB},k}(t)$, the roughly known carrier angular frequency ω_0, and an unknown phase offset $\varphi_{\mathrm{B},k}$. The carrier frequency is only approximately known and, therefore, the beacon's phase $\varphi_{\mathrm{B},k}$ at different time instances is completely independent and unpredictable.

The signal is detected by M base stations, each with I_m antennas, where the ith antenna of the mth base station is located at

$$\vec{p}_{m_i} = (x_{m_i}, y_{m_i}, z_{m_i})^{\mathsf{T}}. \tag{7}$$

At this antenna, the delayed beacon signal

$$s_{m_i,k}(t) = A_{m_i,k} \cdot s_{\mathrm{TX,BB},k}(t - \tau_{m_i,k}) e^{j(\omega_0(t-\tau_{m_i,k})+\varphi_{\mathrm{B},k})}, \tag{8}$$

with the time delay

$$\tau_{m_i,k} = \frac{\left\|\vec{p}_{m_i} - \vec{p}_{\mathrm{B},k}\right\|_2}{c_0} \tag{9}$$

and amplitude $A_{m_i,k}$, is detected. Here, c_0 denotes the speed of light. In order to evaluate the signal's phase, it is mixed with a complex valued local oscillator signal $s_{\mathrm{LO},m}(t)$ with amplitude $A_{\mathrm{LO},m}$, angular frequency $\omega_m \approx \omega_0$, and phase $\varphi_{\mathrm{LO},m,k}$ resulting in the signal

$$\begin{aligned} s_{\mathrm{mix},m_i,k}(t) &= s_{m_i,k}(t) \cdot s_{\mathrm{LO},m}(t) \\ &= A_{m_i,k} \cdot s_{\mathrm{TX,BB},k}(t - \tau_{m_i,k}) \cdot e^{j(\omega_0(t-\tau_{m_i,k})+\varphi_{\mathrm{B},k})} \\ &\quad \cdot A_{\mathrm{LO},m} \cdot e^{-j(\omega_m t+\varphi_{\mathrm{LO},m,k})} \\ &= A_{m_i,k} \cdot A_{\mathrm{LO},m} \cdot s_{\mathrm{TX,BB},k}(t - \tau_{m_i,k}) \\ &\quad \cdot e^{j((\omega_0-\omega_m)t-\omega_0\tau_{m_i,k}+\varphi_{\mathrm{B},k}-\varphi_{\mathrm{LO},m,k})} \\ &\overset{(a)}{=} A_{m_i,k} \cdot A_{\mathrm{LO},m} \cdot e^{j\left(-\omega_0\tau_{m_i,k}+\varphi_{\mathrm{mix},m,k}\right)}. \end{aligned} \tag{10}$$

At (a), for the kth measurement, the signal is sampled at $t = kT_{\mathrm{S}}$, with T_{S} as the sample interval. At this sample instance, the frequency difference $\omega_0 - \omega_m$ and the bandlimited signal $s_{\mathrm{TX,BB},k}(kT_{\mathrm{S}} - \tau_{m_i,k}) \approx s_{\mathrm{TX,BB},k}(kT_{\mathrm{S}} - \tau_{m_j,k})$ result in phase shifts that are the same for every antenna and are included into $\varphi_{\mathrm{mix},m,k}$, eliminating the dependency of t. Generally, it may be beneficial to combine several samples to increase the signal-to-noise ratio. Since these contain different phase shifts, the measurements at the antenna pairs should be directly correlated to evaluate their phase difference, as in [26]. In this paper, only one sample with one unknown phase shift is assumed to provide a consistent description in the following.

Because of the phase ambiguity, from here on, all phases are mapped elementwise to the interval $(-\pi, \pi]$ with

$$\mathrm{mod}'_{2\pi}(\bullet) = \begin{cases} \mathrm{mod}_{2\pi}(\bullet) & \text{for } \mathrm{mod}_{2\pi}(\bullet) < \pi, \\ \mathrm{mod}_{2\pi}(\bullet) - 2\pi & \text{for } \mathrm{mod}_{2\pi}(\bullet) > \pi. \end{cases} \tag{11}$$

The resulting phase $\varphi_{m_i,k} = \mathrm{mod}'_{2\pi}(-\omega_0\tau_{m_i,k} + \varphi_{\mathrm{mix},m,k})$ will be measured. The resulting receive phases of the mth

array are combined to the measurement vector

$$\vec{\varphi}_{m,k} = \mathrm{mod}'_{2\pi}\left(\begin{pmatrix} -\omega_0\tau_{m_1,k} \\ \vdots \\ -\omega_0\tau_{m_I,k} \end{pmatrix} + \begin{pmatrix} \varphi_{\mathrm{mix},m,k} \\ \vdots \\ \varphi_{\mathrm{mix},m,k} \end{pmatrix}\right). \tag{12}$$

Given the measurement (12), the straightforward approach would be to estimate the beacon's position $\vec{p}_{\mathrm{B},k}$ and the unknown incoherent phases for each array $\varphi_{\mathrm{mix},m,k}$ such that the conducted measurement matches the hypothesis in a least squares sense. However, commonly used wavelengths in communication and localization frequency bands range from millimeters to centimeters. Hence, the resulting optimization problem becomes challenging because of the 2π phase ambiguity.

To avoid a computationally expensive and error-prone brute-force search, the phase differences for selected antenna pairs are evaluated. For this purpose, the phases are preprocessed by multiplying the measurement vector with an evaluation matrix $\boldsymbol{A}_m \in \mathbb{R}^{D\times I_m}$ and mapping the result again to $(-\pi, \pi]$ to eliminate artifacts due to the 2π jumps. The number of evaluated phase differences D can be varied depending on the setup, as will be discussed later. In $\boldsymbol{A}_m$, the dth row comprises the entry 1 in the j_dth column and the entry -1 in the i_dth column to evaluate the phase difference between the i_dth and the j_dth antenna, while all other entries are zero. For example, the matrix

$$\boldsymbol{A}_{m,\mathrm{example}} = \begin{bmatrix} 1 & -1 & 0 & 0 \\ 0 & 1 & -1 & 0 \\ 1 & 0 & 0 & -1 \end{bmatrix} \tag{13}$$

evaluates the phase differences of an array consisting of four antennas between the antenna pairs 1–2, 2–3, and 1–4. As a result, the incoherent phase $\varphi_{\mathrm{mix},m,k}$ in (12) cancels out, yielding the new measurement equation

$$\begin{aligned} &\Delta\vec{\varphi}_{m,k} \\ &\quad= \mathrm{mod}'_{2\pi}\left(\boldsymbol{A}_m\vec{\varphi}_{m,k}\right) \\ &\quad= \mathrm{mod}'_{2\pi}\left(\boldsymbol{A}_m\begin{pmatrix} -\omega_0\tau_{m_1,k} \\ \vdots \\ -\omega_0\tau_{m_{I_m},k} \end{pmatrix} + \boldsymbol{A}_m\begin{pmatrix} \varphi_{\mathrm{mix},m,k} \\ \vdots \\ \varphi_{\mathrm{mix},m,k} \end{pmatrix}\right) \\ &\quad= \mathrm{mod}'_{2\pi}\begin{pmatrix} \omega_0(\tau_{m_{j_1},k} - \tau_{m_{i_1},k}) \\ \vdots \\ \omega_0(\tau_{m_{j_D},k} - \tau_{m_{i_D},k}) \end{pmatrix}. \end{aligned} \tag{14}$$

Note that here the modulo mapping of $\vec{\varphi}_{m,k}$ in (12) is redundant because $\boldsymbol{A}_m$ only contains integer numbers.

The number of rows D in $\boldsymbol{A}_m$ as well as their composition should be varied to satisfy different purposes. Because of the incoherent measurement, only $I_m - 1$ phase differences have to be evaluated. Hence, a matrix $\boldsymbol{A}_m$ of rank $I_m - 1$, resulting in a spanning tree [29] between all antennas, is sufficient to maintain all information. The Appendix A provides a more detailed discussion. Note that in the case of very noisy environments or erroneous measurements, it may be favorable to evaluate more than $I_m - 1$ phase differences to cope with errors caused by phase ambiguity. Beside the elimination of the unknown incoherent phase, the usage of phase differences allows a clear allocation of the individual measurements to a certain purpose. Phase differences obtained from closely spaced antenna pairs result in low measurement sensitivity, but a high unambiguity range, whereas distant antenna pairs yield a small unambiguity range but high sensitivity, as depicted in Fig. 3.

Generally, many error sources such as multipath, thermal noise, or oscillator phase noise superpose in practical measurement scenarios. For indoor localization systems, multipath propagation represents the main challenge. To enable computationally efficient least-squares-based localization, the superposition of all error sources is modeled as normally distributed additive noise that is assumed to be uncorrelated between all antennas, as the actual noise correlation properties are unknown. Since this uncorrelated noise assumption is incorrect for multipath propagation, it is beneficial to use receiver arrays with large apertures, thereby decorrelating the line of sight from the multipath propagation [13]. Then, the noisy measured phases of the mth array can be written as

$$\vec{\varphi}_{m,k,\mathrm{noise}} = \mathrm{mod}'_{2\pi}\left(\vec{\varphi}_{m,k} + \vec{n}_{m,k}\right), \tag{15}$$

with $\vec{n}_{m,k} \sim \mathcal{N}(0, \sigma_\varphi^2\boldsymbol{I})$, where σ_φ is the standard deviation of the measurement setup. In accordance with (14), the noisy phase differences are calculated as

$$\Delta\vec{\varphi}_{m,k,\mathrm{noise}} = \mathrm{mod}'_{2\pi}\left(\Delta\vec{\varphi}_{m,k} + \boldsymbol{A}_m\vec{n}_{m,k}\right). \tag{16}$$

By calculating the phase differences, the uncorrelated noise in (15) becomes correlated, yielding the covariance matrix as

$$\boldsymbol{R}_m = \sigma_\varphi^2 \cdot \boldsymbol{A}_m\boldsymbol{A}_m^{\mathsf{T}}. \tag{17}$$

Finally, to combine the measurements of multiple receivers, all $\vec{\varphi}_{m,k}$ are stacked to a vector $\vec{\varphi}_k = (\vec{\varphi}_{1,k}, \ldots, \vec{\varphi}_{M,k})^{\mathsf{T}}$, the noise vectors are stacked as $\vec{n}_k = (\vec{n}_{1,k}, \ldots, \vec{n}_{M,k})^{\mathsf{T}}$, the noisy measurements are stacked as $\vec{\varphi}_{k,\mathrm{noise}} = (\vec{\varphi}_{1,k,\mathrm{noise}}, \ldots, \vec{\varphi}_{M,k,\mathrm{noise}})^{\mathsf{T}}$, and all $\boldsymbol{A}_m$ are stacked as

$$\boldsymbol{A} = \begin{bmatrix} \boldsymbol{A}_1 & 0 & \cdots & 0 \\ 0 & \boldsymbol{A}_2 & & \vdots \\ \vdots & & \ddots & 0 \\ 0 & \cdots & 0 & \boldsymbol{A}_M \end{bmatrix}, \tag{18}$$

which results in the measurement equation

$$\vec{h}(\vec{p}_{\mathrm{B},k}) = \mathrm{mod}'_{2\pi}\left(\boldsymbol{A}\vec{\varphi}_k\right) \tag{19}$$

and the noisy measurement

$$\vec{z}(\vec{p}_{\mathrm{B},k}) = \mathrm{mod}'_{2\pi}\left(\boldsymbol{A}\vec{\varphi}_{k,\mathrm{noise}}\right), \tag{20}$$

as well as the combined measurment noise covariance matrix

$$\boldsymbol{R} = \begin{bmatrix} \boldsymbol{R}_1 & 0 & \cdots & 0 \\ 0 & \boldsymbol{R}_2 & & \vdots \\ \vdots & & \ddots & 0 \\ 0 & \cdots & 0 & \boldsymbol{R}_M \end{bmatrix}. \tag{21}$$

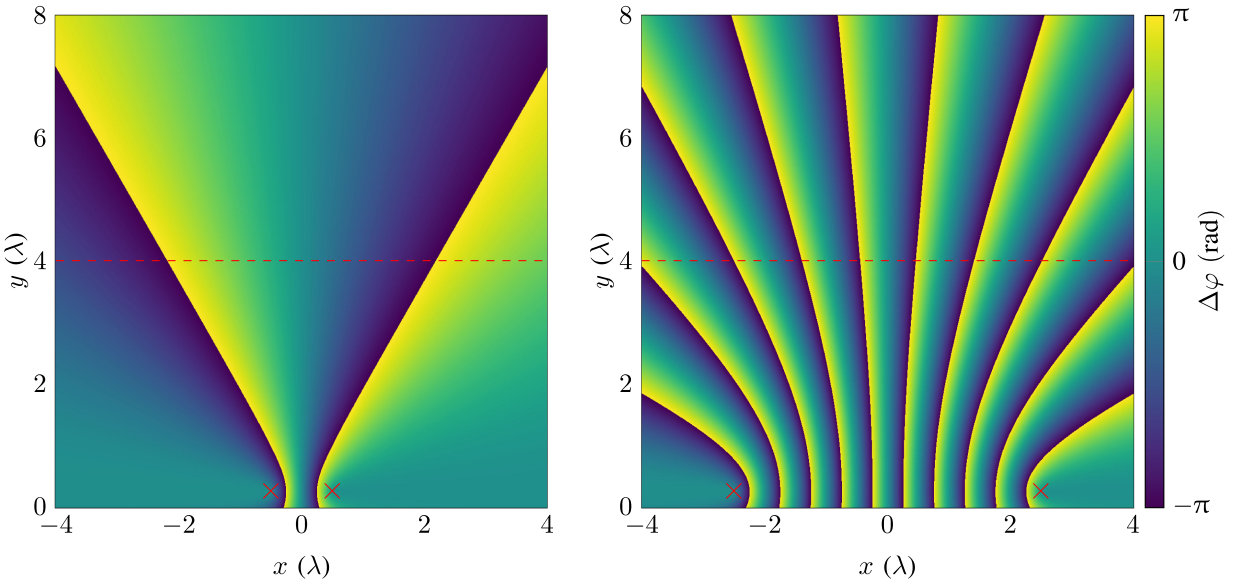

(a) Antenna spacing $1\,\lambda$ (b) Antenna spacing $5\,\lambda$

FIGURE 3. **Emitter position depending phase difference between the receivers, which are marked as red crosses, as well as the line used for the illustration in Fig. 4 in red.**

IV. POSITION ESTIMATION

Generally, a Kalman filter recursively combines the apriori information from the previous measurements via a state prediction with the information of the current measurement. The iterated extended Kalman filter (IEKF) combines the information by iteratively linearizing the measurement model at the current best estimate and solves the originating generalized least squares problem, as in [30]. In this section, the IEKF concept is extended to an iterative evaluation of varying antennas pairs, depending on their distance and, therefore, their unambiguity range. For this purpose, the equations of the IHEKF are derived simultaneously with a discussion on the phase difference ambiguity, thereby enabling a stable convergence to the position estimate. In the following, $\vec{x}_k$ denotes the true state of the system, consisting of the position and velocity, whereas $\vec{x}_{k|k-1}$ denotes the prediction, which is then combined with the measurement to calculate the state update $\vec{x}_{k|k}$. The starting state $\vec{x}_{0|0}$ is assumed to be approximately known. In the following, $\vec{z}(\vec{x}_k)$ and $\vec{h}(\vec{x}_k)$ will be used as the straightforward and trivial extensions of $\vec{z}(\vec{p}_{\mathrm{B},k})$ and $\vec{h}(\vec{p}_{\mathrm{B},k})$ to the complete state $\vec{x}_k$, which includes position and velocity. Note that the measurements only contain information about the current position, while the velocity is estimated indirectly via the movement model.

A. PREDICTION

Since the state transition model as defined in Section III-A is linear, the prediction of the standard Kalman filter (KF) can be used [31]. The prediction for the current state, including the position and speed for every dimension, is calculated as

$$\vec{x}_{k|k-1} = \boldsymbol{F}\vec{x}_{k-1|k-1}, \tag{22}$$

with $\boldsymbol{F}$ as the state transition matrix. Because of the prediction step, the uncertainty, represented by the noise covariance $\boldsymbol{\Sigma}_{k|k-1}$, increases to

$$\boldsymbol{\Sigma}_{k|k-1} = \boldsymbol{F}\,\boldsymbol{\Sigma}_{k-1|k-1}\,\boldsymbol{F}^{\mathsf{T}} + \boldsymbol{Q}, \tag{23}$$

with $\boldsymbol{Q} = \sigma_a^2 \boldsymbol{G}\boldsymbol{G}^{\mathsf{T}}$ as the movement model's noise covariance matrix.

B. MAXIMUM A POSTERIORI COST FUNCTION

Given the prior state prediction and the current measurement $\vec{z}_k$, the beacon is localized by a maximum a posteriori estimation [32] starting from the state prediction. The a posteriori guess is calculated as

$$\vec{x}_{k|k} = \mathrm{argmax}_{\vec{x}_k}\left(p(\vec{x}_k|\vec{z}_k, \vec{x}_{k|k-1})\right), \tag{24}$$

which can be transformed via Bayes' theorem as

$$\begin{aligned}\vec{x}_{k|k} &= \mathrm{argmax}_{\vec{x}_k}\left(\frac{p(\vec{z}_k|\vec{x}_k)\cdot p(\vec{x}_k|\vec{x}_{k|k-1})}{p(\vec{z}_k|\vec{x}_{k|k-1})}\right)\\ &= \mathrm{argmax}_{\vec{x}_k}\left(p(\vec{z}_k|\vec{x}_k)\cdot p(\vec{x}_k|\vec{x}_{k|k-1})\right),\end{aligned} \tag{25}$$

where $p(\vec{z}_k|\vec{x}_{k|k-1})$ normalizes the position–dependent probability to one and can be neglected.

$p(\vec{x}_k|\vec{x}_{k|k-1})$ denotes the probability density function from the prediction step as

$$\begin{aligned}&p(\vec{x}_k|\vec{x}_{k|k-1})\\ &\quad= \frac{1}{\sqrt{\det(2\pi\,\boldsymbol{\Sigma}_{k|k-1})}}\\ &\quad\cdot\exp\left[-\frac{1}{2}(\vec{x}_k-\vec{x}_{k|k-1})^{\mathsf{T}}\boldsymbol{\Sigma}_{k|k-1}^{-1}(\vec{x}_k-\vec{x}_{k|k-1})\right].\end{aligned} \tag{26}$$

$p(\vec{z}_k|\vec{x}_k)$ denotes the probability density function of the kth measurement according to (20). These measurements are

impaired by the phases' 2π ambiguity, which prevents a direct comparison between the measurements and hypothesis. To cope with this 2π ambiguity, the deviation between the measurements and hypothesis is mapped to $(-\pi, \pi]$, thereby implicitly defining the maximal displacement of the predicted beacon position, which can be corrected within the state update. This topic will be further examined in Section IV-C. To study the emerging probability density function, the deviation, defined symmetrically between $(-\pi, \pi]$, is evaluated as

$$\begin{aligned}\text{deviation} &= \text{mod}'_{2\pi}\left(\vec{z}(\vec{x}_k) - \vec{h}(\vec{x}_k)\right)\\ &= \text{mod}'_{2\pi}\left(\text{mod}_{2\pi}\left(\boldsymbol{A}\vec{\varphi}_k + \boldsymbol{A}\vec{n}_k\right) - \text{mod}_{2\pi}\left(\boldsymbol{A}\vec{\varphi}_k\right)\right)\\ &\overset{(a)}{=} \text{mod}'_{2\pi}\left(\boldsymbol{A}\vec{\varphi}_k + \boldsymbol{A}\vec{n}_k - \boldsymbol{A}\vec{\varphi}_k\right)\\ &= \text{mod}'_{2\pi}\left(\boldsymbol{A}\vec{n}_k\right)\\ &\overset{(b)}{=} \boldsymbol{A}\vec{n}_k, \end{aligned} \tag{27}$$

where at (a) the inner $\text{mod}'_{2\pi}$ is redundant and at (b) the phase noise is assumed to be small enough to satisfy $|\boldsymbol{A}\vec{n}_k| < \pi$. This allows an approximation of the measurement probability density function via a normal distribution as

$$\begin{aligned} p(\vec{z}_k|\vec{x}_k) &\approx \frac{1}{\sqrt{2\pi\,\det(\boldsymbol{R})}}\exp\left[-\frac{1}{2}\left(\text{mod}'_{2\pi}(\vec{z}_k - \vec{h}(\vec{x}_k))\right)^{\mathsf{T}}\right.\\ &\qquad \left.\boldsymbol{R}^{-1}\left(\text{mod}'_{2\pi}(\vec{z}_k - \vec{h}(\vec{x}_k))\right)\right]\\ &= \frac{1}{\sqrt{2\pi\,\det(\boldsymbol{R})}}\exp\left[-\frac{1}{2}\vec{\text{res}}_k^{\mathsf{T}}\boldsymbol{R}^{-1}\vec{\text{res}}_k\right], \end{aligned} \tag{28}$$

with the measurement residual $\vec{\text{res}}_k = \text{mod}'_{2\pi}(\vec{z}_k - \vec{h}(\vec{x}_k))$. Inserting (26) and (28) in (25) results in a cost function of the maximum a posteriori estimation

$$\begin{aligned}\vec{x}_{k|k} &= \text{argmax}_{\vec{x}_k}\left(\frac{1}{\sqrt{2\pi\,\det(\boldsymbol{R})}}\exp\left[-\frac{1}{2}\vec{\text{res}}_k^{\mathsf{T}}\,\boldsymbol{R}^{-1}\vec{\text{res}}_k\right]\right.\\ &\qquad \cdot\frac{1}{\sqrt{\det(2\pi\,\boldsymbol{\Sigma}_{k|k-1})}}\\ &\qquad \left.\exp\left[-\frac{1}{2}(\vec{x}_k - \vec{x}_{k|k-1})^{\mathsf{T}}\boldsymbol{\Sigma}_{k|k-1}^{-1}(\vec{x}_k - \vec{x}_{k|k-1})\right]\right)\\ &\overset{(a)}{=} \text{argmin}_{\vec{x}_k}\left(\frac{1}{2}\vec{\text{res}}_k^{\mathsf{T}}\,\boldsymbol{R}^{-1}\vec{\text{res}}_k\right.\\ &\qquad \left.+\frac{1}{2}(\vec{x}_k - \vec{x}_{k|k-1})^{\mathsf{T}}\boldsymbol{\Sigma}_{k|k-1}^{-1}(\vec{x}_k - \vec{x}_{k|k-1})\right)\\ &= \text{argmin}_{\vec{x}_k}\left(J_{\text{meas},k} + J_{\text{pred},k}\right)\\ &= \text{argmin}_{\vec{x}_k}\left(J_k\right), \end{aligned} \tag{29}$$

where at (a) the logarithm as a monotonically increasing function is applied and the minus sign is resolved. The cost function J_k consists of $J_{\text{meas},k} = \frac{1}{2}\vec{\text{res}}_k^{\mathsf{T}}\,\boldsymbol{R}^{-1}\vec{\text{res}}_k$, which represents the influence of the current measurement as well as the prediction part $J_{\text{pred},k} = \frac{1}{2}(\vec{x}_k - \vec{x}_{k|k-1})^{\mathsf{T}}\boldsymbol{\Sigma}_{k|k-1}^{-1}(\vec{x}_k - \vec{x}_{k|k-1})$, which incorporates the prediction from the previous step.

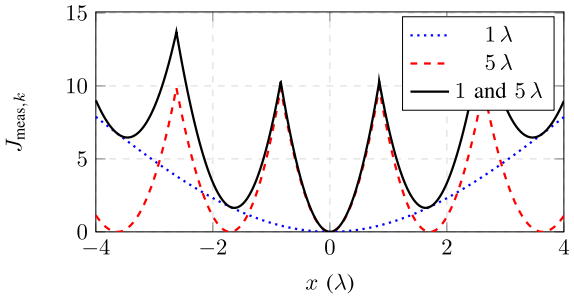

FIGURE 4. $J_{\text{meas},k}$ in (29) for the two antenna arrangements in Fig. 3 with antenna distance of 1 λ and 5 λ as well as their combination for a measurement $\vec{z} = \vec{0}$, depicted for an evaluation along the red line in Fig 3.

C. SOLUTION OF THE MAXIMUM A POSTERIORI COST FUNCTION

As already mentioned in Section IV-B, the measurements' phase ambiguity is resolved by mapping the measurement deviation to $(-\pi, \pi]$ and updating the predicted beacon position within this unambiguity range. In this way, the unambiguity range $(-\pi, \pi]$ implicitly provides the information about the maximally allowed displacement of the predicted beacon position. In the cost function of the maximum a posteriori estimator (29), this is reflected in the non-convex measurement part $J_{\text{meas},k}$, which has, apart from its global minima, multiple local minima due to the 2π phase ambiguity, while the prediction part $J_{\text{pred},k}$ is a quadratic function. To discuss the ambiguity problem in more detail, a closer look is taken at the measurement residual, caused by a wrongly estimated beacon position. First, at time instance k, we assume the beacon is located at a distance $y = d_{\text{array-beacon}}$ directly in front of a receive array at $x = 0$ (e.g. at the center of the dashed red line in Fig. 3 for $d_{\text{array-beacon}} = 4\,\lambda$) and that this estimate is only correct in the y-dimension. The true beacon position in the x-dimension is given by $x_{\text{B},k}$ and directly corresponds to a positioning error in the x-dimension ϵ_x. Now we consider one specific entry of the residual $\vec{\text{res}}_k$, denoted res, which corresponds to a phase difference of two antennas at $y = 0$ with distance d_{ant}. The measurement sensitivity of the residual regarding the position deviation ϵ_x is then approximated in [13] as

$$\frac{\partial \text{res}}{\partial \epsilon_x} \approx \frac{2\pi}{\lambda}\frac{d_{\text{ant}}}{d_{\text{array-beacon}}}, \tag{30}$$

where λ denotes the wavelength of the carrier frequency. Hence, the measurement sensitivity increases with the antenna distance, showing that large arrays are favorable for more precise localization. However, to prevent the divergence to a wrong minimum, the residuum must not be greater than π. Therefore, the deviation between the predicted and real position has to satisfy

$$\epsilon_x < \frac{\pi}{\frac{\partial \text{res}}{\partial x}} \approx \frac{\lambda}{2}\frac{d_{\text{array-beacon}}}{d_{\text{ant}}}. \tag{31}$$

As a consequence, an algorithm that converges reliably towards the global minimum becomes challenging for large arrays. This relationship is visualized in Fig. 4. Here, the

measurement part $J_{\text{meas},k} \sim \text{res}^2$ for the receive antenna pair with distance 5 λ provides a very sensitive but ambiguous error function. In comparison, the error function for the receive antenna pair with distance 1 λ provides a less sensitive but unambiguous error function. The combination of both measurements yields a distinct minimum with a high measurement sensitivity. However, due to the antenna pair with 5 λ distance, the combined error function is not convex, thereby hindering phase-based localization concepts as the HEKF. To deal with this issue and support the algorithm's convergence to the global minimum, the state estimation is subdivided into $i_{\max}$ iterations, denoted with a superscript i. In each iteration, the involved antenna pairs are varied by adapting the evaluation matrix of the ith iteration $\boldsymbol{A}^i$. Hence, $\vec{z}_k^i$, $\vec{h}_k^i$, $\boldsymbol{R}_k^i$, and $\vec{\text{res}}_k^i$ also change their size in each iteration.

In the first iteration, when the prior guess of the position, represented by the state prediction $\vec{x}_{k|k}^0 = \vec{x}_{k|k-1}$, is vague, only closely spaced antenna pairs with a high unambiguity range but low measurement sensitivity are evaluated, yielding the more accurate state estimation $\vec{x}_{k|k}^1$. Since the involvement of further measurement data improves the state estimation accuracy and, hence, reduces phase difference ambiguity issues, the IHEKF iteratively involves the phase differences of more distant antenna pairs in the following. Finally, the IHEKF stops when a full spanning tree is created at each receiver to include all information, as discussed in Section III and the Appendix. To perform one iteration of the proposed IHEKF, the measurement function is linearized around the current best guess $x_{k|k}^i$, yielding

$$\begin{aligned}
&\text{mod}'_{2\pi}\left(\vec{z}_k^i - \vec{h}^i(\vec{x}_k)\right) \\
&\quad = \text{mod}'_{2\pi}\left(\vec{z}_k^i - \vec{h}^i(\vec{x}_{k|k}^i) - \boldsymbol{H}^i \cdot (\vec{x}_k - \vec{x}_{k|k}^i)\right) \\
&\quad \overset{(a)}{=} \text{mod}'_{2\pi}\left(\vec{z}_k^i - \vec{h}^i(\vec{x}_{k|k}^i)\right) - \boldsymbol{H}^i \cdot (\vec{x}_k - \vec{x}_{k|k}^i), \qquad (32)
\end{aligned}$$

with the Jacobi matrix

$$\boldsymbol{H}^i = \frac{\partial \vec{h}^i(\vec{x}_k)}{\partial \vec{x}_k}\Big|_{\vec{x}_{k|k}^i}. \qquad (33)$$

At (a), the extraction of $\boldsymbol{H}^i \cdot (\vec{x}_k - \vec{x}_{k|k}^{i-1})$ from the $\text{mod}_{2\pi}(\cdot)$ function is only possible as long as the current state prediction $x_{k|k}^i$ does not cause ambiguity issues. Inserting (32) in (29) results in

$$\begin{aligned}
\vec{x}_{k|k}^{i+1} = \text{argmin}_{\vec{x}_k} &\left(\frac{1}{2}\left(\text{mod}'_{2\pi}\left(\vec{z}_k^i - \vec{h}^i(\vec{x}_{k|k}^i)\right)\right.\right. \\
&\left.-\boldsymbol{H}_k^i \cdot (\vec{x}_k - \vec{x}_{k|k}^i)\right)^{\mathsf{T}} \\
&\boldsymbol{R}_k^{i\,-1}\left(\text{mod}'_{2\pi}\left(\vec{z}_k^i - \vec{h}^i(\vec{x}_{k|k}^i)\right) - \boldsymbol{H}_k^i \cdot (\vec{x}_k - \vec{x}_{k|k}^i)\right) \\
&\left.+\frac{1}{2}(\vec{x}_k - \vec{x}_{k|k-1})^{\mathsf{T}}\boldsymbol{\Sigma}_{k|k-1}^{-1}(\vec{x}_k - \vec{x}_{k|k-1})\right) \\
= \text{argmin}_{\vec{x}_k}&\left(J_k^i\right). \qquad (34)
\end{aligned}$$

To solve (34), the derivative of J_k^i is required. With the identity $\frac{\partial((\boldsymbol{A}\vec{x}+\vec{b})^{\mathsf{T}}\boldsymbol{C}(\boldsymbol{A}\vec{x}+\vec{b}))}{\partial \vec{x}} = 2\boldsymbol{A}^{\mathsf{T}}\boldsymbol{C}(\boldsymbol{A}\vec{x}+\vec{b})$ for $\boldsymbol{C} = \boldsymbol{C}^{\mathsf{T}}$ from [33, p. 11], the first derivative is calculated as

$$\begin{aligned}
\text{grad}(J_k^i) = &\boldsymbol{H}_k^{i\,\mathsf{T}}\boldsymbol{R}_k^{i\,-1}\left(\text{mod}'_{2\pi}\left(\vec{z}_k^i - \vec{h}^i(\vec{x}_{k|k}^i)\right)\right. \\
&\left.+\boldsymbol{H}_k^i(\vec{x}_k - \vec{x}_{k|k}^i)\right) + \boldsymbol{\Sigma}_{k|k-1}^{-1}(\vec{x}_k - \vec{x}_{k|k-1}). \qquad (35)
\end{aligned}$$

By setting $\text{grad}(J_k^i) = \vec{0}$, the next state estimate is obtained as

$$\begin{aligned}
x_{k|k}^{i+1} = &\left(\boldsymbol{H}_k^{i\,\mathsf{T}}\boldsymbol{R}_k^{i\,-1}\boldsymbol{H}_k^i + \boldsymbol{\Sigma}_{k|k-1}^{-1}\right)^{-1} \\
&\left(\boldsymbol{H}_k^{i\,\mathsf{T}}\boldsymbol{R}_k^{i\,-1}\left(\text{mod}'_{2\pi}\left(\vec{z}_k^i - \vec{h}^i(\vec{x}_{k|k}^i)\right)\right.\right. \\
&\left.\left.+\boldsymbol{H}_k^i\vec{x}_{k|k}^i\right) + \boldsymbol{\Sigma}_{k|k-1}^{-1}\vec{x}_{k|k-1}\right) \\
= &\boldsymbol{K}_k^i\left(\text{mod}'_{2\pi}\left(\vec{z}_k^i - \vec{h}^i(\vec{x}_{k|k}^i)\right)\right. \\
&\left.+\boldsymbol{H}_k^i\vec{x}_{k|k}^i\right) + (\boldsymbol{I} - \boldsymbol{K}_k^i\boldsymbol{H}_k^i)\vec{x}_{k|k-1} \\
= &\vec{x}_{k|k-1} + \boldsymbol{K}_k^i\left(\text{mod}'_{2\pi}\left(\vec{z}_k^i - \vec{h}^i(\vec{x}_{k|k}^i)\right)\right. \\
&\left.-\boldsymbol{H}_k^i\left(\vec{x}_{k|k}^i - \vec{x}_{k|k-1}\right)\right) \qquad (36)
\end{aligned}$$

with

$$\left(\boldsymbol{H}_k^{i\,\mathsf{T}}\boldsymbol{R}_k^{i\,-1}\boldsymbol{H}_k^i + \boldsymbol{\Sigma}_{k|k-1}^{-1}\right)^{-1} = \left(\boldsymbol{I} - \boldsymbol{K}_k^i\boldsymbol{H}_k^i\right)\boldsymbol{\Sigma}_{k|k-1}, \qquad (37)$$

and the Kalman gain

$$\begin{aligned}
\boldsymbol{K}_k^i &= (\boldsymbol{H}_k^{i\,\mathsf{T}}\boldsymbol{R}_k^{i\,-1}\boldsymbol{H}_k^i + \boldsymbol{\Sigma}_{k|k-1}^{-1})^{-1}\boldsymbol{H}_k^{i\,\mathsf{T}}\boldsymbol{R}_k^{i\,-1} \\
&= \boldsymbol{\Sigma}_{k|k-1}\boldsymbol{H}_k^{i\,\mathsf{T}}(\boldsymbol{R}_k^i + \boldsymbol{H}_k^i\boldsymbol{\Sigma}_{k|k-1}\boldsymbol{H}_k^{i\,\mathsf{T}})^{-1}, \qquad (38)
\end{aligned}$$

which can be found in [30]. After the final iteration, the state is updated as $x_{k|k} = x_{k|k}^i$ and the covariance matrix can be calculated similar to [31] as

$$\boldsymbol{\Sigma}_{k|k} = (\boldsymbol{I} - \boldsymbol{K}_k^i\boldsymbol{H}_k^i)\boldsymbol{\Sigma}_{k|k-1}. \qquad (39)$$

Note that the resulting equations are similar to the IEKF equations [30] except for the $\text{mod}'_{2\pi}$ function and the variation of the evaluated phase differences via $\boldsymbol{A}^i$.

D. DISCUSSION OF THE RESULTING IHEKF

To enable highly accurate PDOA–based localization, large antenna arrays are necessary to provide high measurement sensitivity and suppress the influence of multipath propagation [13]. For this purpose, the evaluation of the relative phase information of widely spaced antennas is necessary. However, the phase difference measurements of largely spaced antenna arrays are impaired by severe ambiguity issues. To solve this issue, this paper proposes the IHEKF in Algorithm I, which is created via the previously established equations.

In (40) and (41), the IHEKF's prediction step, which does not differ from a standard KF, is conducted. Then the beacon is localized using the IHEKF's iterative estimation procedure in (44)-(49), starting from the predicted state $\vec{x}_{k|k}^0 = \vec{x}_{k|k-1}$ in (43). In each iteration, the evaluation matrix $\boldsymbol{A}^i$ is adapted

Algorithm 1 Holographic Iterated Extended Kalman Filter

1. Prediction:

$$\vec{x}_{k|k-1} = \boldsymbol{F}\,\vec{x}_{k-1|k-1} \tag{40}$$

$$\boldsymbol{\Sigma}_{k|k-1} = \boldsymbol{F}\,\boldsymbol{\Sigma}_{k-1|k-1}\,\boldsymbol{F}^{\mathsf{T}} + \boldsymbol{Q}_k \tag{41}$$

2. Iteration:

$$i = 0 \tag{42}$$

$$\vec{x}^{0}_{k|k} = \vec{x}_{k|k-1} \tag{43}$$

while $i < i_{\max}$ **do:**

$$\vec{z}^{\,i}_k = \boldsymbol{A}^i \cdot \vec{\varphi}_{k,\text{noise}} \tag{44}$$

$$\boldsymbol{R} = \sigma_\varphi^2 \cdot \boldsymbol{A}^i \boldsymbol{A}^{i\mathsf{T}} \tag{45}$$

$$\boldsymbol{H}^i_k = \frac{\partial\, \vec{h}^{\,i}(\vec{x_k})}{\partial\, \vec{x_k}}\Big|_{\vec{x}^{\,i}_{k|k}} \tag{46}$$

$$\boldsymbol{K}^i_k = \boldsymbol{\Sigma}_{k|k-1}\boldsymbol{H}^{i\mathsf{T}}_k(\boldsymbol{R}^i_k + \boldsymbol{H}^i_k\boldsymbol{\Sigma}_{k|k-1}\boldsymbol{H}^{i\mathsf{T}}_k)^{-1} \tag{47}$$

$$\vec{x}^{\,i+1}_{k|k} = \vec{x}^{\,i}_{k|k} + \boldsymbol{K}^i_k\left(\text{mod}'_{2\pi}\left(\vec{z}^{\,i}_k - \vec{h}^{\,i}\left(\vec{x}^{\,i}_{k|k}\right)\right) - \boldsymbol{H}^i_k\left(\vec{x}^{\,0}_{k|k} - \vec{x}^{\,i}_{k|k}\right)\right) \tag{48}$$

$$i = i + 1 \tag{49}$$

end while

3. Update:

$$\vec{x}_{k|k} = \vec{x}^{\,i}_{k|k} \tag{50}$$

$$\boldsymbol{\Sigma}_{k|k} = (\boldsymbol{I} - \boldsymbol{K}^i_k\,\boldsymbol{H}^i_k)\boldsymbol{\Sigma}_{k|k-1} \tag{51}$$

to successively include the phase measurement of more distant antennas, which represents the key idea of the proposed algorithm. For this purpose, we suggest initializing $\boldsymbol{A}^0$ by solely evaluating the phase differences of the most closely spaced antenna pairs. Since the state $\vec{x}^{\,1}_{k|k}$, which is estimated using $\boldsymbol{A}^0$, is a better estimate for the correct position, it is thereafter possible to include the phase differences of more distant antennas without creating an ambiguity issue. Thus, the full spanning tree within each antenna array, which is necessary to include all information as discussed in Section IV-B, is created by iteratively adding the antennas closest to the current spanning tree, while in each iteration the state estimate $\vec{x}^{\,i}_{k|k}$ is improved and, hence, ambiguity issues diminish. Note that although the phase differences of the most distant antenna pairs are not directly evaluated within the spanning tree, the IHEKF implicitly evaluates these phase differences via the intermediate antennas due to the cross-correlation entries in the correlation matrix $\boldsymbol{R}^i_k$. In doing so, the spanning tree further severely reduces ambiguity issues in comparison to the direct evaluation of the most distant antennas. To perform one iteration the measured phase differences are evaluated first in (44). Then the noise covariance matrix $\boldsymbol{R}^i_k$ of the current preprocessing matrix $\boldsymbol{A}^i$ is computed in (45). Using the linearized system model in (46) and the Kalman gain in (47), the next best guess is estimated in (48). After $i_{\max}$ iterations, the state and its covariance are updated in (50) and (51), respectively.

The computational complexity of extended Kalman filters (EKFs) depends on the size of the state vector L_x with $\text{O}(L_\text{x}^2)$ and particularly on the size of the measurement vector L_z, which determines the dimension and, as a consequence, the complexity of the matrix inversion [31, p. 43]. The scaling of the complexity of the matrix inversion depends on the matrix size itself and is $\text{O}(L_\text{z}^{2.807})$ for medium–sized matrices [34]. In comparison, the IEKF performs $i_{\max}$ iterations and, hence, the complexity increases to $\text{O}(i_{\max}L_\text{z}^{2.807})$. However, the proposed IHEKF varies the number of evaluated phase differences $L_{\text{z},i}$ in every iteration i, and therefore the complexity reduces to $\text{O}(\sum_{i=1}^{i_{\max}} {L_{\text{z},i}}^{2.807})$. Altogether, although the IHEKF performs several iterations for one update step, the computational complexity only slightly increases in comparison to a state update with a single iteration.

In summary, the resulting Algorithm I enables reliable, highly accurate, and computationally efficient PDOA-based localization by evaluating the phase differences between the antennas of large receiver arrays. For this purpose, the phase differences at each receiver are evaluated via an iteratively increasing spanning tree, which enables the evaluation of distant antenna pairs via intermediate antennas, to combine the ambiguity information of closely spaced antennas and the high measurement sensitivity of large receiver apertures. Since no requirements on the beacon's waveform are made, the IHEKF represents a valuable candidate for the accurate localization in communication standards such as 5G/6G.

V. EXPERIMENTAL VERIFICATION

In this section, the proposed IHEKF is verified. First, a real world setup is described and four different algorithm variants are introduced. Then the results for one simple and one complex trajectory are shown to evaluate the capability and demonstrate the superiority of the IHEKF over the HEKF under real world influences, such as multipath propagation and antenna crosstalk.

A. MEASUREMENT SETUP AND ALGORITHM VARIANTS

As shown in Fig. 5, three 24 GHz base stations are placed in a room with about 1 m distance between each of them, facing towards the midpoint 2 m beneath them. Similarly to bearings-only localization systems, the positions and orientations of the base stations were chosen such that the geometric dilution of precision [35] is optimized. Each base station evaluates the phases of 10 receive antennas, which create the 254 mm x 91 mm aperture depicted in Fig. 6 with the corresponding spanning tree. Note that the receivers in Fig. 5 contain more than 10 antennas; These are not necessary for the content of this paper and are not used. The beacon, which emits a 24 GHz signal, is mounted on a robotic arm that maneuvers the emitter and provides a reference position to evaluate the IHEKF's localization results. Each array has been calibrated in-situ, as proposed in [36].

FIGURE 5. Hardware setup consisting of a 24 GHz CW-transmitter (TX) mounted on a precise robotic arm, as well as three receivers (RX) mounted on the ceiling.

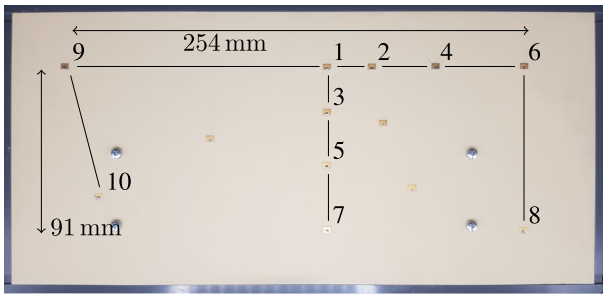

FIGURE 6. This is one of the three identical antenna arrays used in the experimental setup shown in Fig. 5. It has a size of 254 mm x 91 mm with a minimum antenna distance of 2 λ between antenna 1 and 2 and a maximum antenna distance of 21.6 λ between antenna 8 and 9, as well as the spanning tree, which is used for the evaluation with all 10 antennas. The unmarked antennas are not used for the presented evaluation.

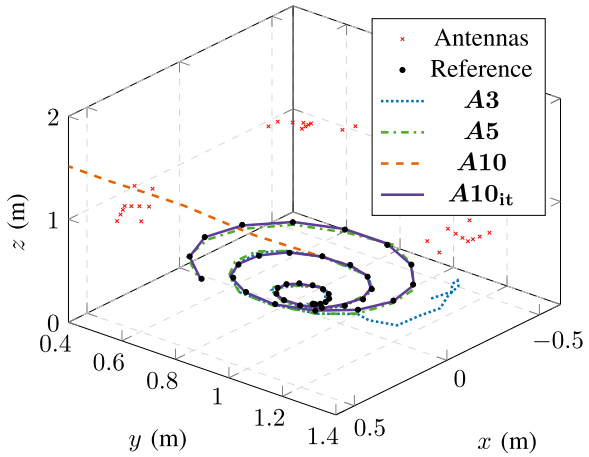

FIGURE 7. Localization results for the spiral trajectory using the four different evaluation algorithms $A3$, $A5$, $A10$, and $A10_{it}$.

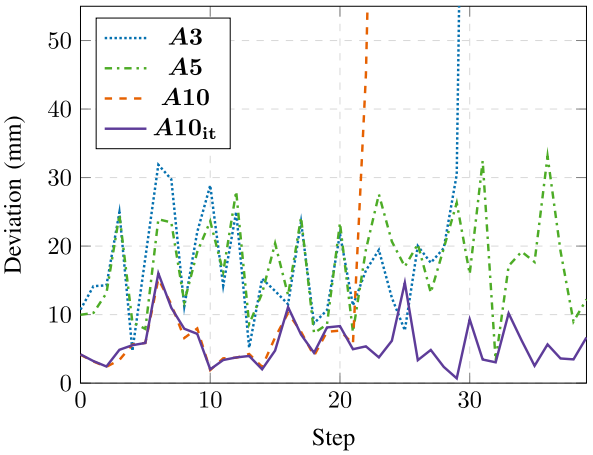

FIGURE 8. Deviation of the localization results for the spiral trajectory in Fig. 7.

To verify the IHEKF and enable an intuitive understanding of the IHEKF's behavior, the four different algorithms ***A3***, ***A5***, ***A10***, and $\boldsymbol{A10}_{\text{it}}$ are used to localize the beacon. While ***A3***, ***A5***, and ***A10*** estimate the beacon's position without iterating, $\boldsymbol{A10}_{\text{it}}$ uses three iterations with different matrix sizes, i.e. with different numbers of evaluated phase differences. The first two algorithms are intended to demonstrate the IHEKF's capability for resolving the phase ambiguity via the spanning tree, which is created by the evaluation matrix. ***A3*** solely evaluates the phase differences between antennas 1, 4, and 5, thereby omitting antennas 2 and 3 in the spanning tree in Fig. 6. Since the sole evaluation of these distant antennas 1, 4, and 5 is prone to phase ambiguity errors, ***A5*** includes antennas 2 and 3 such that 1, 4, and 5 are only indirectly connected via the spanning tree. To increase measurement sensitivity, ***A10*** includes all remaining antennas in Fig. 6. However, this includes the phase difference evaluation of distant antenna pairs and thus is prone to ambiguity issues. To prevent such issues, $\boldsymbol{A10}_{\text{it}}$ uses the IHEKF and thereby evaluates the phase measurements of antennas 1, 2, and 3 in the first iteration, includes the measurements of antennas 4 and 5 in the second iteration, and then finally estimates the beacon's position using all antennas.

For comparison, the root-mean-square-error (RMSE) is calculated by

$$\text{RMSE} = \sqrt{\frac{\sum_{k=1}^{k_{\max}} \left\| \vec{p}_{\text{B},k} - \vec{p}_{\text{B},k}^{\,\text{est}} \right\|_2^2}{k_{\max}}}, \tag{52}$$

where $\vec{p}_{\text{B},k}^{\,\text{est}}$ denotes the estimated beacon positions and $k_{\max}$ the total number of steps.

B. MEASUREMENT RESULTS

First, the measurements, which belong to the spiral trajectory depicted in Fig. 7, are evaluated. The spiral trajectory is designed so that the distances between the beacon's positions continuously increase. Therefore, the localization of the shown trajectory becomes increasingly difficult and is well suited to assess the algorithms' performance.

The first algorithm ***A3*** is able to localize the beacon during the first, closely spaced trajectory positions. However, as visible in Fig. 8, which shows the deviation per measurement,

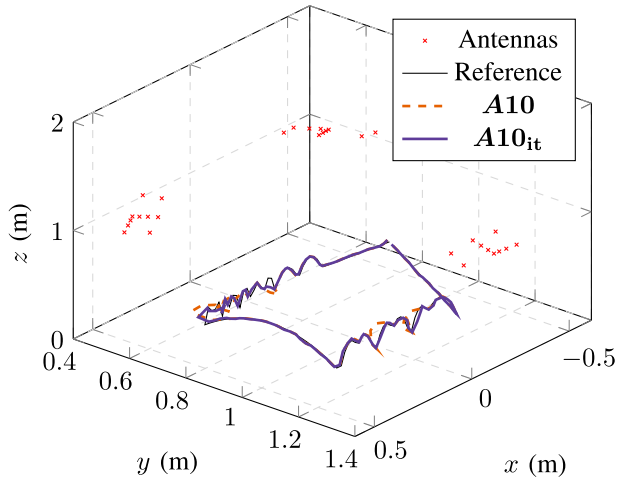

FIGURE 9. Localization results for a complex trajectory the two evaluation algorithms $A10$ and $A10_{\text{it}}$.

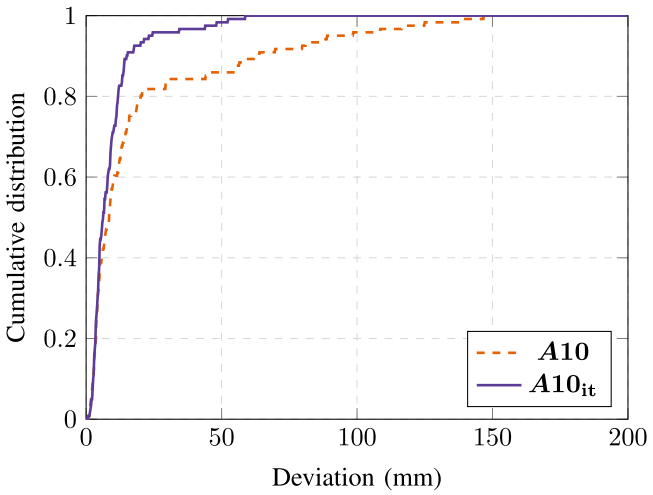

FIGURE 10. Cumulative distribution of the deviation from the trajectory in Fig. 9.

A3 diverges at step 29. In comparison, ***A5*** includes antennas 2 and 3 to prevent ambiguity issues, yielding approximately the same accuracy as ***A3*** at the beginning, but allows reliable tracking over the full trajectory. Algorithm ***A10***, which evaluates the phase measurements of all antennas in a single iteration to increase measurement sensitivity, provides highly accurate localization results during the first steps. However, ***A10*** diverges at step 22 due to ambiguous measurements at the distant antennas 8, 9, and 10. To prevent this, $\boldsymbol{A10}_{\text{it}}$ performs three iterations to successively include more antennas, thereby enabling highly accurate localization throughout the whole trajectory and yields a RMSE of 5.7 mm.

To further illustrate the capabilities of the IHEKF, a second trajectory, consisting of $k_{\max} = 121$ positions, is driven, which strongly differs from the constant velocity model. For the sake of clarity, only the results of ***A10*** and $\boldsymbol{A10}_{\text{it}}$ are shown in Fig. 9. The corresponding cumulative error distributions are shown in Fig. 10. Here, ***A10*** struggles when the trajectory does not match the constant velocity assumption, since this causes the position prediction to strongly differ from the true beacon position. The filter does not diverge due to the high sampling rate. In comparison, $\boldsymbol{A10}_{\text{it}}$ can precisely track the complete trajectory, yielding a RMSE of 9.0 mm.

VI. CONCLUSION

In this paper, the IHEKF was presented, which enables highly accurate PDOA-based localization using large antenna arrays. Since virtually no requirements concerning the beacon have to be met, the IHEKF is particularly suited for accurate localization within existing communication systems such as WIFI, BT, and 5G/6G. Nevertheless, there remain several open topics for future research. First, an algorithm initialization for an unknown beacon position is necessary. Different approaches are possible and optimal candidates should be identified for specific applications. Furthermore, the IHEKF so far assumes constant and known noise variances. Hence, an adaptive noise estimation would be beneficial in practice, which would also enable the detection of non-line-of-sight conditions.

APPENDIX

In this Appendix, it is shown that the evaluation of $I_m - 1$ phase differences in the mth array using the preprocessing matrix A_m is sufficient to contain all information about the beacon's position.

For this purpose, we use

$$\boldsymbol{A}'_m = \begin{bmatrix} \boldsymbol{A}_m \\ \hline \boldsymbol{A}_{m,\text{abs}} \end{bmatrix} \in \mathbb{R}^{I_m \times I_m}, \tag{53}$$

with $\boldsymbol{A}_m \in \mathbb{R}^{I_m - 1 \times I_m}$, which has rank $I_m - 1$ and evaluates $I_m - 1$ phase differences, and $\boldsymbol{A}_{m,\text{abs}} \in \mathbb{R}^{1 \times I_m}$, which evaluates one absolute phase. For example, $\boldsymbol{A}'_m$ might be

$$\boldsymbol{A}'_m = \begin{bmatrix} 1 & 0 & 0 & \cdots & 0 & -1 \\ 0 & 1 & 0 & \cdots & 0 & -1 \\ 0 & 0 & 1 & \cdots & 0 & -1 \\ \vdots & \vdots & \vdots & \ddots & \vdots & \\ 0 & 0 & 0 & \cdots & 1 & -1 \\ \hline 0 & 0 & 0 & \cdots & 0 & -1 \end{bmatrix}. \tag{54}$$

This yields

$$\begin{aligned} \begin{pmatrix} \Delta\vec{\varphi}_{m,k} \\ \hline -\varphi'_{m_i,k} \end{pmatrix} &= \text{mod}'_{2\pi}\left(\boldsymbol{A}'_m \vec{\varphi}_{m,k}\right) \\ &= \text{mod}'_{2\pi}\left(\boldsymbol{A}'_m \begin{pmatrix} \varphi_{m_1,k} \\ \vdots \\ \varphi_{m_I,k} \end{pmatrix} + \begin{pmatrix} 0 \\ \vdots \\ 0 \\ \hline -\varphi_{\text{mix},m,k} \end{pmatrix}\right) \\ &\overset{(a)}{=} \boldsymbol{A}'_m \begin{pmatrix} \varphi_{m_1,k} \\ \vdots \\ \varphi_{m_I,k} \end{pmatrix} + \begin{pmatrix} 0 \\ \vdots \\ 0 \\ \hline -\varphi_{\text{mix},m,k} \end{pmatrix} + \begin{pmatrix} d_1 \cdot 2\pi \\ \vdots \\ d_{I_m} \cdot 2\pi \end{pmatrix}, \end{aligned} \tag{55}$$

where at (a) the $\mathrm{mod}'_{2\pi}$ is rewritten as an addition of $d_i \cdot 2\pi$, with d_i chosen, so that the result is mapped to $(-\pi, \pi]$. Since this is an affine transformation (linear transformation followed by a translation) with full rank, no information is lost. While in the first $I_m - 1$ rows the unknown phase $\varphi_{\mathrm{mix},m,k}$ is shortened, $\varphi_{\mathrm{mix},m,k}$ is subtracted in the last row. However, $\varphi_{\mathrm{mix},m,k}$ is unknown and, hence, the last row does not contain any information about the beacon's position and can be omitted.

REFERENCES

[1] M. Vossiek, L. Wiebking, P. Gulden, J. Wieghardt, C. Hoffmann, and P. Heide, "Wireless local positioning," *IEEE Microw. Mag.*, vol. 4, no. 4, pp. 77–86, Dec. 2003.

[2] F. Zafari, A. Gkelias, and K. K. Leung, "A survey of indoor localization systems and technologies," *IEEE Commun. Surv. Tutor.*, vol. 21, no. 3, pp. 2568–2599, Jul.–Sep. 2019.

[3] Y. Dobrev, M. Vossiek, M. Christmann, I. Bilous, and P. Gulden, "Steady delivery: Wireless local positioning systems for tracking and autonomous navigation of transport vehicles and mobile robots," *IEEE Microw. Mag.*, vol. 18, no. 6, pp. 26–37, 2017.

[4] H. Liu, H. Darabi, P. Banerjee, and J. Liu, "Survey of wireless indoor positioning techniques and systems," *IEEE Trans. Syst. Man Cybern., Part C. Appl. Rev.*, vol. 37, no. 6, pp. 1067–1080, Sep./Oct. 2007.

[5] S. Mazuelas *et al.*, "Robust indoor positioning provided by real-time RSSI values in unmodified WLAN networks," *IEEE J. Sel. Top. Signal Proces.*, vol. 3, no. 5, pp. 821–831, Oct. 2009.

[6] H. L. van Trees, *Optimum Array Processing: Part IV of Detection, Estimation, and Modulation Theory*. Hoboken, NJ, USA: Wiley, 2002.

[7] R. M. Vaghefi and R. M. Buehrer, "Asynchronous time-of-arrival-based source localization," in *Proc. IEEE Int. Conf. Acoust. Speech Signal Process*, 2013, pp. 4086–4090.

[8] C. Zhang, M. Kuhn, B. Merkl, A. E. Fathy, and M. Mahfouz, "Accurate UWB indoor localization system utilizing time difference of arrival approach," in *Proc. IEEE Radio Wireless Symp.*, 2006, pp. 515–518.

[9] T. Ussmueller, D. Brenk, J. Essel, J. Heidrich, G. Fischer, and R. Weigel, "Roundtrip-time-of-flight based localization of passive multi-standard RFID-tags," in *Proc. IEEE Int. Conf. Wireless Inf. Technol. Syst.*, 2012, pp. 1–4.

[10] A. M. Ladd, K. E. Bekris, A. Rudys, L. E. Kavraki, and D. S. Wallach, "Robotics-based location sensing using wireless ethernet," *Wireless Netw.*, vol. 11, no. 1, pp. 189–204, 2005.

[11] S. Roehr, P. Gulden, and M. Vossiek, "Method for high precision clock synchronization in wireless systems with application to radio navigation," in *Proc. IEEE Radio Wireless Symp.*, 2007, pp. 551–554.

[12] A. R. J. Ruiz and F. S. Granja, "Comparing ubisense, bespoon, and decawave uwb location systems: Indoor performance analysis," *IEEE Trans. Instrum. Meas.*, vol. 66, no. 8, pp. 2106–2117, Aug. 2017.

[13] E. Sippel, J. Geiss, S. Brückner, P. Gröschel, M. Hehn, and M. Vossiek, "Exchanging bandwidth with aperture size in wireless indoor localization - or why 5G/6G systems with antenna arrays can outperform UWB solutions," *IEEE Open J. Veh. Technol.*, vol. 2, pp. 207–217, 2021.

[14] A. Alarifi *et al.*, "Ultra wideband indoor positioning technologies: Analysis and recent advances," *Sensors*, vol. 16, no. 5, p. 707, 2016.

[15] S. Gezici *et al.*, "Localization via ultra-wideband radios: A look at positioning aspects for future sensor networks," *IEEE Signal Process. Mag.*, vol. 22, no. 4, pp. 70–84, Jul. 2005.

[16] C. Zhang, M. J. Kuhn, B. C. Merkl, A. E. Fathy, and M. R. Mahfouz, "Real-time noncoherent UWB positioning radar with millimeter range accuracy: Theory and experiment," *IEEE Trans. Microw. Theory Tech.*, vol. 58, no. 1, pp. 9–20, Jan. 2009.

[17] C. Meier, A. Terzis, and S. Lindenmeier, "A robust 3D high precision radio location system," in *Proc. IEEE/MTT-S Int. Microw. Symp.*, 2007, pp. 397–400.

[18] M. R. Mahfouz, C. Zhang, B. C. Merkl, M. J. Kuhn, and A. E. Fathy, "Investigation of high-accuracy indoor 3-D positioning using UWB technology," *IEEE Trans. Microw. Theory. Tech.*, vol. 56, no. 6, pp. 1316–1330, Jun. 2008.

[19] D. Dardari, A. Conti, U. Ferner, A. Giorgetti, and M. Z. Win, "Ranging with ultrawide bandwidth signals in multipath environments," *Proc. IEEE*, vol. 97, no. 2, pp. 404–426, Feb. 2009.

[20] S. Cao, Y. F. Zheng, and R. L. Ewing, "From phased array to holographic radar," in *Proc. IEEE Nat. Aerosp. Electron. Conf.*, 2015, pp. 207–212.

[21] A. J. Fenn, D. H. Temme, W. P. Delaney, and W. E. Courtney, "The development of phased-array radar technology," *Linc. Lab. J.*, vol. 12, no. 2, pp. 321–340, 2000.

[22] T. Pavlenko, C. Reustle, Y. Dobrev, M. Gottinger, L. Jassoume, and M. Vossiek, "Design and optimization of sparse planar antenna arrays for wireless 3-D local positioning systems," *IEEE Trans. Antennas Propag.*, vol. 65, no. 12, pp. 7288–7297, Dec. 2017.

[23] M. Lipka *et al.*, "Wireless 3D localization concept for industrial automation based on a bearings only extended Kalman filter," in *Proc. IEEE Asia-Pacific Microw. Conf.*, 2018, pp. 821–823.

[24] A. Miller and B. Miller, "Underwater target tracking using bearing-only measurements," *J. Commun. Technol. Electron.*, vol. 63, no. 6, pp. 643–649, 2018.

[25] M. Hehn, E. Sippel, and M. Vossiek, "An iterative extended kalman filter for coherent measurements of incoherent network nodes in positioning systems," *IEEE Access*, vol. 8, pp. 36 714–36 727, 2020.

[26] M. Lipka, E. Sippel, and M. Vossiek, "An extended Kalman filter for direct, real-time, phase-based high precision indoor localization," *IEEE Access*, vol. 7, pp. 25 288–25 297, 2019.

[27] H. Yin, D. Gesbert, M. Filippou, and Y. Liu, "A coordinated approach to channel estimation in large-scale multiple-antenna systems," *IEEE J. Sel. Areas Commun.*, vol. 31, no. 2, pp. 264–273, Feb. 2013.

[28] E. G. Larsson, O. Edfors, F. Tufvesson, and T. L. Marzetta, "Massive MIMO for next generation wireless systems," *IEEE Commun. Mag.*, vol. 52, no. 2, pp. 186–195, Feb. 2014.

[29] P. Wright, "On minimum spanning trees and determinants," *Math. Mag.*, vol. 73, no. 1, pp. 21–28, 2000.

[30] B. M. Bell and F. W. Cathey, "The iterated Kalman filter update as a gauss-newton method," *IEEE Trans. Automat. Control*, vol. 38, no. 2, pp. 294–297, Feb. 1993.

[31] D. F. Sebastian Thrun and W. Burgard, *Probabilistic Robotics*. Cambridge, MA, USA: MIT Press, 2005.

[32] T. D. Barfoot, *State Estimation for Robotics*. Cambridge, U.K.: Cambridge Univ. Press, 2017.

[33] K. B. Petersen and M. S. Pedersen, *The Matrix Cookbook.* Toronto, ON, Canada: Univ. Waterloo, Nov. 2012.

[34] M. Raitoharju and R. Piché, "On computational complexity reduction methods for Kalman filter extensions," *IEEE Aerosp. Electron. Syst. Mag.*, vol. 34, no. 10, pp. 2–19, Oct. 2019.

[35] Y. Zhong, X. Y. Wu, and S. C. Huang, "Geometric dilution of precision for bearing-only passive location in three-dimensional space," *Electron. Lett.*, vol. 51, no. 6, pp. 518–519, 2015.

[36] E. Sippel, M. Lipka, J. Geiß, M. Hehn, and M. Vossiek, "In-situ calibration of antenna arrays within wireless locating systems," *IEEE Trans. Antennas Propag.*, vol. 68, no. 4, pp. 2832–2841, Apr. 2020.

STEFAN BRÜCKNER was born in Kronach, Germany, in 1992. He received the M.Sc. degree in electronic engineering in 2019 from Friedrich-Alexander-Universität Erlangen–Nürnberg (FAU), Erlangen, Germany, where he is currently working toward the Ph.D. degree. In 2019, he joined the Institute of Microwaves and Photonics, FAU. His current research interests include radar for close range applications, indoor positioning, Kalman filter for localization, and signal processing.

ERIK SIPPEL was born in Fürth, Germany, in 1991. He received the M.Sc. degree in electronic engineering in 2015 from Friedrich-Alexander-Universität Erlangen–Nürnberg (FAU), Erlangen, Germany, where he is currently working toward the Ph.D. degree. In 2016, he joined the Institute of Microwaves and Photonics, FAU. His current research interests include indoor localization, especially radar for near-field localization, data transmission, and analog-to-digital conversion.

MELANIE LIPKA received the M.Sc. degree in electronic engineering and the Ph.D. degree from Friedrich Alexander-Universität Erlangen–Nürnberg (FAU), Erlangen, Germany, in 2014 and 2021, respectively. In 2015, she joined the Institute of Microwaves and Photonics, FAU. In 2021, she joined the Group for Satellite Based Localization, Fraunhofer Institute for Integrated Circuits (IIS), where she is currently researching antennas for localization tasks. Her research interests include radar for close range applications, indoor positioning, Kalman filter for localization, and signal processing.

JOHANNA GEISS (Graduate Student Member, IEEE) was born in Lich, Germany, in 1992. She received the master's degree in electrical engineering in 2017 from Friedrich-Alexander-Universität Erlangen–Nürnberg (FAU), Erlangen, Germany, where she is currently working toward the Ph.D. degree with the Institute of Microwaves and Photonics (LHFT). She is primarily working in the fields of radar signal processing and calibration, radar-based localization, and ego-motion estimation.

MARTIN VOSSIEK (Fellow, IEEE) received the Ph.D. degree from Ruhr-Universität Bochum, Bochum, Germany, in 1996. In 1996, he joined Siemens Corporate Technology, Munich, Germany, where he was the Head of the Microwave Systems Group, from 2000 to 2003. Since 2003, he has been a Full Professor with Clausthal University, Clausthal-Zellerfeld, Germany. Since 2011, he has been the Chair of the Institute of Microwaves and Photonics (LHFT), Friedrich-Alexander-Universität Erlangen–Nürnberg, Erlangen, Germany. He has authored or coauthored more than 300 articles. His research has led to more than 90 granted patents. His current research interests include radar, transponder, RF identification, communication, and wireless locating systems. He is a Member of the German National Academy of Science and Engineering (acatech) and of German Research Foundation (DFG) review board. He is a Member of the German IEEE Microwave Theory and Techniques (MTT)/Antennas and Propagation (AP) Chapter Executive Board and a Member of the IEEE MTT Technical Committees MTT-24 Microwave/mm-wave Radar, Sensing, and Array Systems, MTT-27 Connected and Autonomous Systems (as Founding Chair), MTT- 29 Microwave Aerospace Systems. He is also on the advisory board of the IEEE CRFID Technical Committee on Motion Capture and Localization. He was the recipient of more than ten best paper prices and several other awards. He was awarded the 2019 Microwave Application Award from the IEEE MTT Society (MTT-S) for Pioneering Research in Wireless Local Positioning Systems. He is a Member of organizing committees and technical program committees for many international conferences and he was on the Review Boards for numerous technical journals. From 2013 to 2019, he was an Associate Editor for the IEEE TRANSACTIONS ON MICROWAVE THEORY AND TECHNIQUES.